ENVIRONMENTAL RESEARCH
LETTERS

LETTER • OPEN ACCESS

Greening vs browning? Surface water cover mediates how tundra and boreal ecosystems respond to climate warming

ENVIRONMENTAL RESEARCH
LETTERS

CrossMark

OPEN ACCESS

RECEIVED
24 March 2021

REVISED
28 August 2021

ACCEPTED FOR PUBLICATION
3 September 2021

PUBLISHED
16 September 2021

LETTER

Greening vs browning? Surface water cover mediates how tundra and boreal ecosystems respond to climate warming

Jing Li[1,2], Milena Holmgren[1,*] and Chi Xu[2,*]

1 Department of Environmental Sciences, Wageningen University, Droevendaalsesteeg 3a, 6708 PB Wageningen, The Netherlands
2 School of Life Sciences, Nanjing University, Nanjing 210023, People's Republic of China
* Authors to whom any correspondence should be addressed.

E-mail: milena.holmgren@wur.nl and xuchi@nju.edu.cn

Keywords: Arctic, climate change, ecological transition, permafrost, sub-Arctic, vegetation dynamics, woody encroachment

Supplementary material for this article is available online

Abstract

Climate warming in northern high latitudes has progressed twice as fast as the global average, leading to prominent but puzzling changes in vegetation structure and functioning of tundra and boreal ecosystems. While some regions are becoming greener, others have lost or shifted vegetation condition as indicated by a browning signal. The mechanisms underlying this 'greening or browning enigma' remain poorly understood. Here we use multi-sourced time-series of satellite-derived vegetation indices to reveal that spectral greening is associated with reductions in surface water cover (i.e. fraction of surface water bodies), whereas spectral browning is linked to increases in surface water cover. These patterns are consistently observed from both 30 m resolution Landsat data and 250 m resolution MODIS data on the basis of grid cells sized of 1, 2 and 4 km. Our study provides, to our knowledge, the first biome-scale demonstration that interactions between vegetation condition and water cover change can explain the contrasting trajectories of ecosystem dynamics across the northern high latitudes in response to climate warming. These divergent trajectories we identified have major implications for ecosystem functioning, carbon sequestration and feedbacks to the climate system. Further unraveling the interaction between vegetation and surface water will be essential if we are to understand the fate of tundra and boreal biomes in a warming climate.

1. Introduction

Northern high latitudes are warming twice as fast as the global average (Pachauri *et al* 2014, Post *et al* 2019). This warming has been linked to changes in permafrost condition (Smith *et al* 2005), hydrology (Walter *et al* 2006), vegetation (Myneni *et al* 1997, Piao *et al* 2020), and disturbance regimes (Guindon *et al* 2018). Disentangling the complex interactions between these abiotic and biotic changes is a fundamental step to anticipate the long-term dynamics of tundra and boreal ecosystems.

Satellite-derived spectral greening (i.e. positive trend in vegetation indices (VIs)) has been one of the most conspicuous changes associated with climate warming in northern high latitudes (Myneni *et al* 1997, Berner *et al* 2020, Myers-Smith *et al* 2020, Piao *et al* 2020). This long-term greening trend has been interpreted as enhanced vegetation growth driven by temperature rise and correlated with changes in vegetation cover (Elmendorf *et al* 2012), biomass (Forbes *et al* 2010), productivity (Berner *et al* 2020), abundance and height (Elmendorf *et al* 2012), as well as prolonged plant growing season (Zeng *et al* 2013, Park *et al* 2016). Comparable trends have been documented by field observations. For example, increased abundance and height of vascular plants have been recorded across permanent plots in the Arctic tundra (Elmendorf *et al* 2012). Also long-term field monitoring has demonstrated increases in shrub biomass, cover, height and abundance, as well as advanced spring phenology, and a northern expansion of shrub distribution ranges in Siberian, Alaskan and northern Canadian tundra (Frost and Epstein 2014). In the boreal biome, spectral greening has been attributed to increased forest productivity (Beck *et al*

2011), to transitions from coniferous to deciduous forests, as well as to a northward shift in the distribution range of trees (Wang and Friedl 2019).

Despite the widespread greening trends in tundra and boreal ecosystems, there is also evidence showing opposite trends of vegetation change inferred from satellite-derived spectral browning (i.e. negative trend in VIs). Although in some cases spectral browning could be at least partly caused by sensor degradation (Guay *et al* 2014), there is much field evidence of vegetation declines across certain areas of tundra and boreal ecosystems (Phoenix and Bjerke 2016). Tree mortality caused by more frequent and intensified wildfires and insect outbreaks explains some of these changes (Gamon *et al* 2013, Bjerke *et al* 2017, National Academies Of Sciences 2019, Wang and Friedl 2019). However, in areas where these disturbances are apparently absent, spectral browning and vegetation decline have been related to winter warming, frost drought and waterlogged conditions by thermokarst development (Phoenix and Bjerke 2016, National Academies Of Sciences 2019).

Although vegetation may recover from extreme winter warming (Bokhorst *et al* 2011) and fire (Bret-Harte *et al* 2013) perturbations, it has been hypothesized that potential positive feedback mechanisms may lead to abrupt and persistent changes in vegetation structure in boreal and tundra ecosystems (Scheffer *et al* 2012). In tundra ecosystems, for example, a well-known feedback involves snow–shrub interactions. The presence of shrubs can augment snow accumulation in winter, raising winter soil temperature and facilitating shrub survival (Sturm *et al* 2001). A substantial loss of shrub cover may therefore disrupt this self-maintenance mechanism and new feedbacks may develop. In both Siberian and Alaskan sites, thawing of ice-rich permafrost resulting from rising summer temperatures can lead to waterlogged conditions resulting in shrub and tree mortality (Osterkamp *et al* 2000, Hinzman *et al* 2005, Karlsson *et al* 2011, Frost and Epstein 2014). Once aboveground woody vegetation decreases, positive feedbacks could potentially unfold to further increase permafrost thawing. Small-scale *in situ* experiments have demonstrated that removal of shrub cover can result in summer thawing of the top permafrost and, in turn, leading to soil subsidence and increases of surface water cover which further facilitate permafrost thawing and prevent the reestablishment of shrubs (Blok *et al* 2010, Nauta *et al* 2015).

Although the abovementioned lines of evidence suggest that surface water cover may play an important role in the complex interactions that determine the direction of vegetation change, there has been yet no global assessment of how changes in surface water cover, vegetation condition and climate interact with each other across northern high latitudes. In this study, we address this gap by examining the relationships between trends in surface water cover and spectral greening and browning across the tundra and boreal biomes during 2000–2015. Building on the results from small-scale *in situ* experiments in tundra (Blok *et al* 2010, Nauta *et al* 2015), we expected that negative associations between the trends in surface water cover and spectral greenness could be detectable at larger spatial scales, and therefore hypothesized that greening trends across high latitude landscapes were likely associated to reductions in surface water cover whereas browning vegetation trends were associated to wetter conditions reflected by increases in surface water cover. For surface water cover, we focused on the inland surface water bodies (e.g. ponds), that can be consistently detected through Landsat images at a resolution of 30 m (Pekel *et al* 2016).

2. Methods

We explore how changes in surface water cover relate with trends in spectral greening and browning (i.e. linear changes in the annual mean of VIs during the growing season) across the tundra and boreal biomes. Using time-series of satellite-derived annual surface water cover (Pekel *et al* 2016) and several VIs (including the normalized difference vegetation index (NDVI) and enhanced vegetation index (EVI), derived from both MODIS and Landsat data), we calculated the temporal trends of spectral greenness and surface water cover between 2000 and 2015 on the basis of grid cells of varying sizes. We used linear regression modeling to examine the bivariate associations between the resulting grid-cell based trends of water cover and spectral greenness. We further used structural equation modeling (SEM) taking into account trends of climate change and topographic conditions to infer how changes in surface water cover and vegetation could interact with each other to explain trends in spectral greening and browning. To account for the potential uncertainties associated with remotely sensed data, trend quantification methodology and spatial heterogeneity, we systematically tested for the robustness to different VIs, different trend indicators, different continents, different biome types, different permafrost conditions, and different observational scales.

2.1. Study area

We defined the study area using the biome map from World Wildlife Fund (Olson *et al* 2001). We extracted the polygons defined as 'tundra' and 'boreal forest/Taiga' in the WWF biome classification system as our study system (45° N–80° N). Before the analyses, we filtered out the areas that are subject to strong human activities using the Global Human Influence Index (HII) version 2 dataset at 1 km resolution (Wildlife Conservation Society—WCS and Center for International Earth Science Information Network—CIESIN—Columbia

University 2005). The HII data values range from 0 to 64 representing an increasing intensity of human activities. We excluded the 1 km grid cells using a HII cutoff of 10, below which areas presenting apparent human land uses and areas in proximity to major roads and railways are mostly excluded, therefore human influences are considered very weak. We excluded the grid cells that intersect with coastlines and major rivers to avoid potential hydrological influences of these large water bodies. We also excluded the burnt areas during 2000–2015 using the MODIS MCD45 Burnt Area data (Giglio *et al* 2015) to avoid potential influences of fire.

2.2. Data sources and pre-processing

We used satellite-derived VIs to quantify vegetation dynamics at the circum-Arctic scale, including NDVI and EVI from the Terra Moderate Resolution Imaging Spectroradiometer (the MODIS MOD13Q1v006 level 3 product generated every 16 d) at a spatial resolution of 250 m (Didan 2015), and the Landsat images at a spatial resolution of 30 m. We adopted these multiple datasets to account for potential bias from single VIs or sensors, especially for high-latitude regions (Myers-Smith *et al* 2020). We selected the MODIS and Landsat data that are available for the study time period 2000–2015. For the MODIS NDVI and EVI data, we first picked up the pixels flagged as 'Good Data' in the Summary Quality layer, and then masked out the water pixels using the MODIS yearly Land Water Mask (MOD44Wv006) product (pixels classified as water in any year between 2000–2015). The Landsat NDVI and EVI were calculated from the atmospherically corrected USGS Landsat 7 Surface Reflectance Tier 1 dataset, where the pixels flagged as 'cloud', 'cloud shadow' or 'snow' in the pixel_qa band were excluded. We also excluded the Landsat pixels classified as water in any year between 2000 and 2015 using the Global Surface Water Dataset (Pekel *et al* 2016). For both MODIS and Landsat VIs, we also masked out the non-vegetated pixels by excluding the pixels consistently presenting VI value below 0.1 across 2000–2015. Through these exclusions we are able to focus on quantifying spectral greenness of terrestrial areas. We then calculated annual mean growing-season (between 1 July and 1 September (Goetz *et al* 2005)), NDVI and EVI per vegetated pixel between 2000 and 2015 as indicators of spectral greenness. To test for the robustness with respect to observational scale, we additionally checked the 3rd generation NDVI data from the Global Inventory Monitoring and Modeling System (GIMMS NDVI3gv1, available for 1981–2013) at a spatial resolution of 8 km for the time period of 2000–2013.

The water cover data were obtained from the Global Surface Water Dataset (Pekel *et al* 2016) derived from Landsat data at 30 m spatial resolution. For the calculation of water cover of each year, we focused on the water bodies that can be consistently identified by all available cloud-free remotely-sensed data in the ice-free season (referred to as 'permanent water' in the Global Surface Water Dataset).

The mean annual temperature (MAT) and mean annual precipitation (MAP) data were obtained from the climate research unit (CRU) at 0.5° spatial resolution (Harris *et al* 2020). We excluded the areas with gap filled precipitation data to account for potential bias (Macias-Fauria *et al* 2014). The permafrost data were obtained from the circum-Arctic permafrost and ground ice map (Brown *et al* 2002) that maps permafrost cover in four categories ('continuous': 90%–100%, 'discontinuous': 50%–90%, 'sporadic': 10%–50%, and 'isolated patches': 0%–10%). In our analyses we combined the categories of 'discontinuous', 'sporadic' and 'isolated patches'. As a result, permafrost conditions in our study area were represented by three categories, i.e. 'continuous permafrost' (90%–100% permafrost cover), 'discontinuous permafrost' (0%–90%), and 'permafrost free'. The elevation data obtained from the USGS Global 30 arc-second Elevation datasets (GTOPO30) were used to derive topographic slope.

2.3. Spatial and statistical analyses

We divided the study area into 1 km $\times$ 1 km grid cells to calculate the mean yearly growing-season NDVI/EVI and percentage cover of permanent surface water within each grid cell. For the subsequent analyses we excluded the grid cells without any surface water cover throughout the study time period of 2000–2015, as we focus on the relationships between surface water cover and vegetation. We used a robust regression approach with the Theil–Sen estimator to determine the slope of the regression as an indicator of temporal trend (on an annual basis) for each variable (i.e. NDVI/EVI, surface water cover, MAT and MAP) per grid cell (figures 1(a), (b) and S1 (available online at stacks.iop.org/ERL/16/104004/mmedia)). We used the non-parametric Mann–Kendall trend test to test if there is significant monotonic increasing or decreasing trend. Considering that noise in the time series may potentially bias the trend estimates, we looked at two additional trend indicators, including signal-to-noise ratio (defined as trend divided by standard deviation of the time series), and significant trend (i.e. retaining the grid cells with $p < 0.1$ from the Mann–Kendall trend test for trends of VIs and surface water cover). We illustrated the distributions of mean NDVI/EVI trend within the state space of MAT/MAP trend against surface water cover trend (at bins sized of 0.003 $^{\circ}\mathrm{C\,yr^{-1}}$ MAT in figure 2(a) and 0.2 $\mathrm{mm\,yr^{-1}}$ MAP in figure 2(b)). To test if the observed patterns are affected by grain size, we conducted multi-scale analyses by going through all abovementioned procedures on the basis of 2 km $\times$ 2 km, 4 km $\times$ 4 km, and 8 km $\times$ 8 km grid cells, respectively. We chose a static grid approach instead of a sliding window approach here.

We conducted a spatial neighborhood analysis to detect spatial associations between ecosystem changes in focal areas and neighboring areas. To quantify the effect of spatial autocorrelation (SA) processes in shaping the detected associations, we constructed SA models assuming (a) no SA, (b) SA generated purely by extrinsic processes (i.e. where the associations between spectral greenness and surface water cover are completely caused by certain spatially structured environmental factors), (c) SA generated purely by intrinsic processes (i.e. where changes of spectral greenness or surface water cover at focal sites can 'spill over' to influence the neighboring sites, causing the associations), and (d) SA generated by both extrinsic and intrinsic processes, respectively (see supplementary materials section S1 and Teng *et al* (2018) for details). If the models assuming existence of intrinsic processes (models 3 or 4) present better performance (assessed by the Akaike information criterion (AIC)), then there plausibly exist spatial interactions between spectral greenness and surface water cover changes. Therefore, these spatial modeling analyses can not only account for the potential influence of SA on model parameter estimation, but also help to infer the potential spatial interactions (Teng *et al* 2018).

We used piecewise SEM to explore potential drivers of the opposite trends of spectral greenness and surface water cover. In the SEM, we included MAT and MAP trends as climatic drivers of spectral greenness and surface water cover trends, that play a major role on how vegetation-water dynamics could respond to a long-term trend of global warming. Because topography affects drainage, we included topographic slope as an influencing factor on surface water cover, and therefore as an indirect driver of vegetation change. Such a minimal SEM is not meant to approach complex causal mechanisms in realistic situations. Instead, with this simplistic consideration, we aimed at testing if the remotely sensed observations are best fit under which one of the three different assumptions of interactions: (a) assuming one-way effect from spectral greenness trend on surface water cover trend, (b) assuming one-way effect from surface water cover trend on spectral greenness trend, and (c) assuming spectral greenness and surface water cover trends affect each other. As piecewise SEMs cannot disentangle feedback loops explicitly, bi-directional relationships are evaluated through simple correlation reflecting that the variables are co-varying. Corresponding with the abovementioned assumptions, we constructed three SEM models with (a) surface water cover trend as responsible variable, (b) spectral greenness trend as responsible variable, and (c) co-varying surface water cover trend and spectral greenness trend. We used simple linear models in the piecewise SEM as the data approach normal distributions. We assessed AIC based on the Fisher's C statistic as the indicator of model performance. The models were fitted for the whole tundra and boreal biomes, as well as for different continents, different biome types, different permafrost conditions, different VIs and different trend indicators separately. Data processing and spatial analyses were conducted with the Google Earth Engine platform (Gorelick *et al* 2017) and ArcGIS 10.2. The SEM was conducted using the R 3.5.3 software (R Core Team 2018) with the piecewiseSEM package (Lefcheck 2016).

3. Results and discussion

3.1. Divergent trends of surface water cover and vegetation

Our analyses show that spectral greening and browning co-occur across high latitude regions where water bodies are present (figure 1). Both spectral greening and browning can also happen as MAT (figure 2(a)) and precipitation change (figure 2(b)). These puzzling patterns reflect the complexity of local tundra and boreal vegetation dynamics in response to climate changes (Myers-Smith *et al* 2020).

Our analysis demonstrates an interesting spatial congruence between opposite trends in surface water cover and vegetation condition reflected by different VIs analyzed (figure 1(c), table S1). This negative correlation becomes even stronger if areas with insignificant temporal changes in these variables are excluded (Mann–Kendall trend test, $p > 0.1$), as seen from a drastic increase of Pearson's correlation coefficients from $\sim$0.2 to $\sim$0.6 (table S1).

By slightly smoothing the VI trends, a clear pattern emerges, namely, we find spectral greening to be strongly associated with reductions in surface water cover, whereas spectral browning is strongly associated with increases in surface water cover (figures 2(a) and (b)). These patterns of greening and browning in relation to opposite trends in surface water cover are highly consistent for both NDVI and EVI derived from MODIS (250 m resolution) and Landsat (30 m resolution) data, and are also robust across regions with contrasting permafrost conditions (i.e. continuous permafrost, discontinuous permafrost, and permafrost-free areas), biome types (i.e. boreal and tundra biomes), and continents (i.e. Eurasia and North America) (figure S2). Interestingly, the patterns are most pronounced at smaller grid cell sizes of 1 and 2 km, and become attenuated at 4 and 8 km (figure S3). Two landscape-scale examples of these patterns can be seen at the Kytalyk site in eastern Siberia, where ecosystem changes are characterized by spectral browning associated to surface water cover increases, and in the Atqasuk site in North America, where spectral greening is associated to decreases in surface water cover (figure S4).

These revealed associated opposite trends between surface water cover and spectral greening and browning could partly be a result of reciprocal

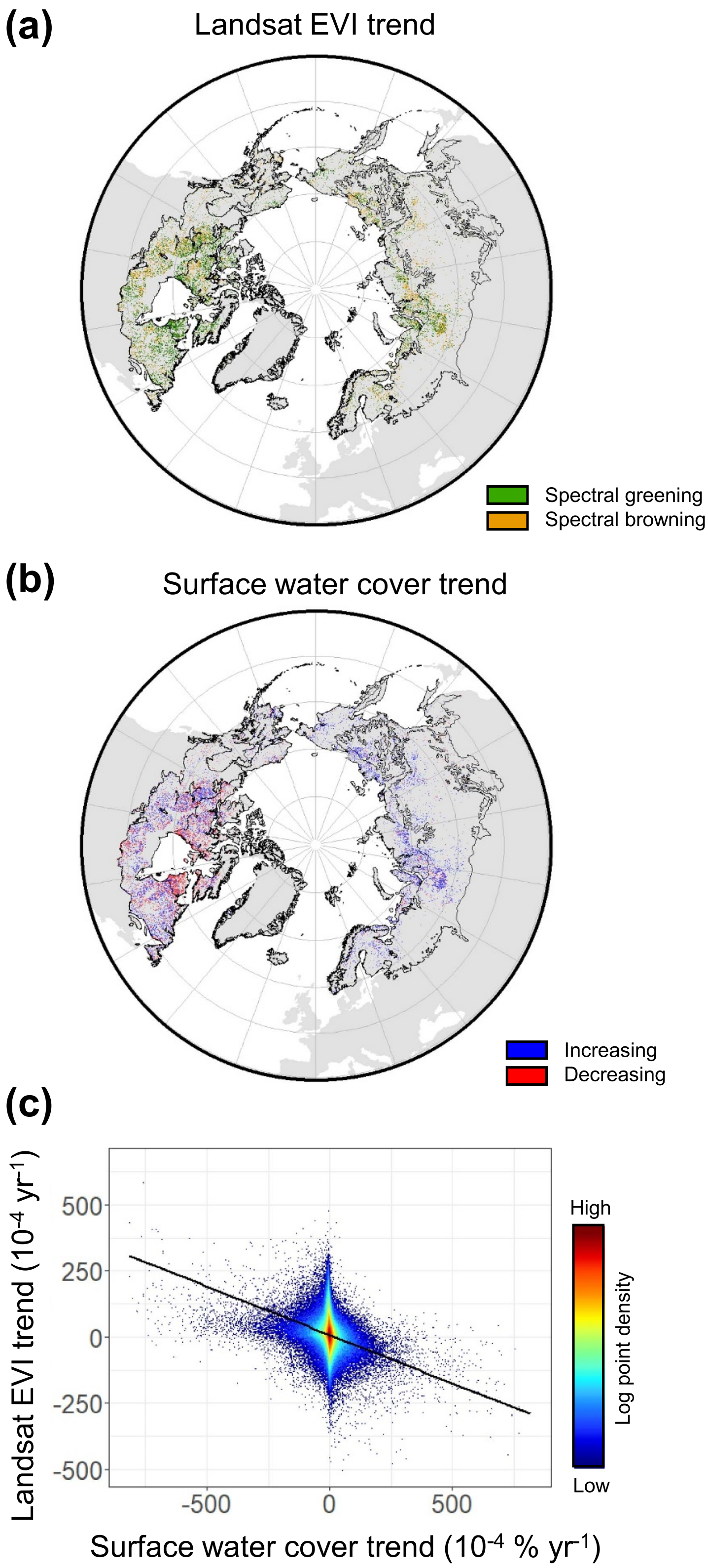

Figure 1. Trends of spectral greenness and surface water cover across the tundra and boreal biomes during 2000–2015. (a) Map of spectral greening and browning reflected as increasing and decreasing Landsat EVI trends respectively at 1 km grid cells. Areas subject to human influences, fire and low-quality of remote sensing data were filtered out (see section 2). (b) Map of increasing and decreasing surface water cover trends calculated using the Global Surface Water Dataset (Pekel *et al* 2016) derived from Landsat data. (c) Spatial congruence between spectral greenness and water cover trends (Pearson's r correlation coefficient of -0.18, $p < 2.2 \times 10^{-16}$, $n = 5191\,139$). The point density and the slope line based on ordinary least square regression are shown (note that the 95% confidence interval is very close to the black solid slope line). The correlation becomes stronger (Pearson's r correlation coefficient of -0.60, $p < 2.2 \times 10^{-16}$, $n = 6886$) if looking at areas with significant trends only. See figure S1 and table S1 for the results based on all four VIs used (i.e. Landsat NDVI and EVI; MODIS NDVI and EVI).

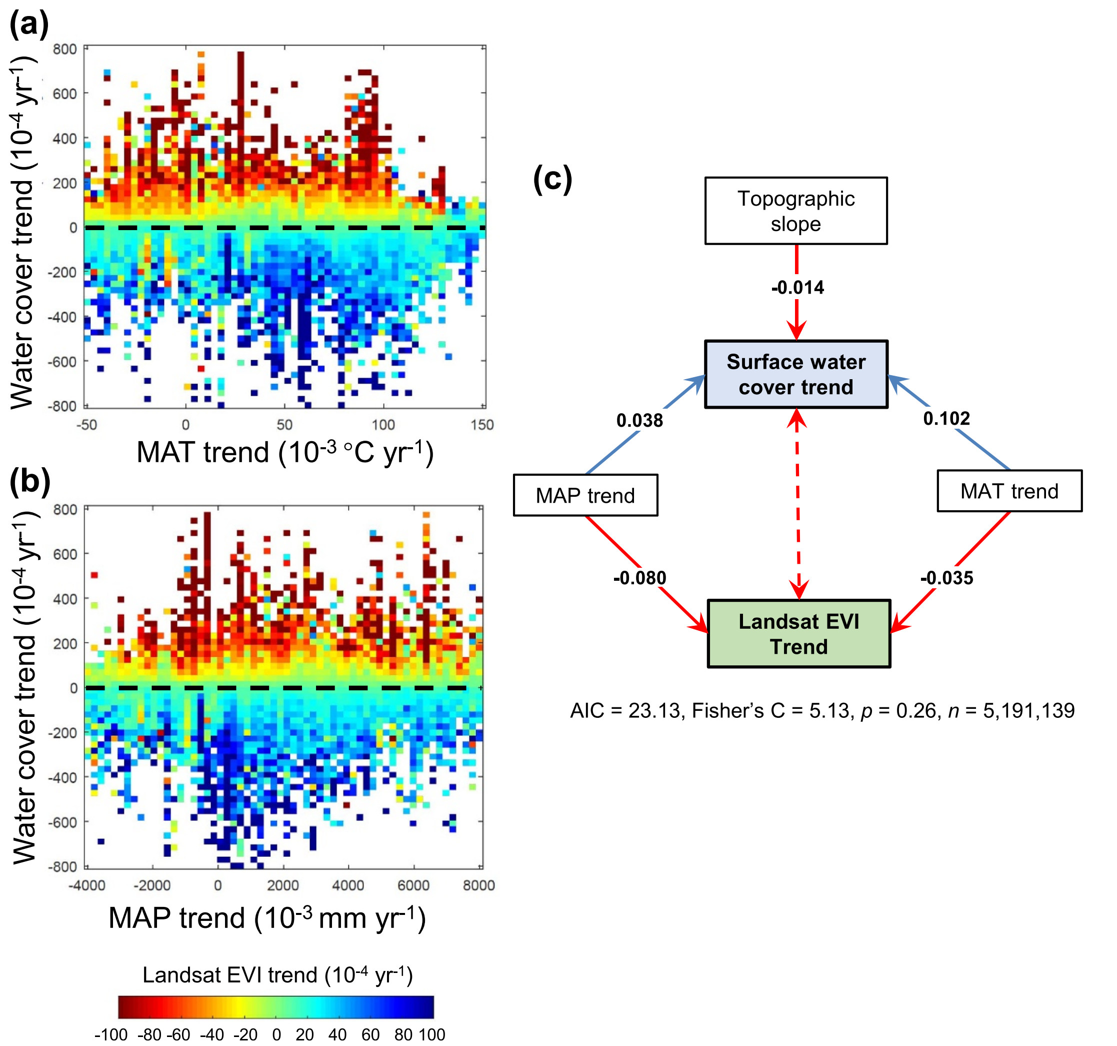

Figure 2. Spectral greenness trends in relation to surface water cover and climatic trends. (a) Distribution of spectral greenness trend in relation to MAT trend as x axis and surface water cover trend (as y axis). (b) Distribution of spectral greenness trend in relation to MAP trend as x axis and surface water cover trend as y axis. (c) A minimal SEM suggests plausible interactions between the trends of surface water cover, spectral greenness and climate. Both spectral greening (positive EVI trend represented by blue dots) and browning (negative EVI trend represented by red dots) can happen when the climate has become warmer or cooler, drier or wetter ((a) and (b)). Interestingly, spectral greening mostly occurs in areas with decreasing surface water cover, whereas browning mostly occurs in areas with increasing water cover ((a) and (b)). The horizontal dashed lines in ((a) and (b)) separate between decreasing surface water cover (negative water cover trend) and increasing surface water cover (positive water cover trend). The model assuming co-varying surface water cover and spectral greenness trends (a bi-directional relationship) is the best fit across the tundra and boreal biomes on a global scale (c). Red and blue arrows indicate negative and positive effects (with their standardized coefficients, $p < 2.2 \times 10^{-16}$ for all effects), respectively. Dashed double-direction red arrow indicates co-variation of spectral greenness trend and surface water cover trend, possibly resulting from their reciprocal feedbacks. For model fitting, bootstrapping was conducted with 1000 repetitions and 50 000 random samples drawn from 51 91 139 data points in each repetition to account for potential influence of SA on parameter estimates. Note here that p values greater than 0.05 indicate satisfactory model performance. Trends of MAT, MAP, spectral greenness and surface water cover in ((a)–(c)) are calculated as slopes (Theil–Sen estimator) of the robust linear regression of these variables against time during 2000–2015, on the basis of 1 km grid cells. The color scale in ((a) and (b)) indicates mean EVI trend within the state space of MAT/MAP trend against surface water cover trend, at bins sized of 0.003 °C yr^{-1} MAT in (a) and 0.2 mm yr^{-1} MAP in (b). See supplementary materials (figures S2, S3 and table S2) for more results for different VIs used (i.e. Landsat NDVI and EVI; MODIS NDVI and EVI), continents (i.e. Eurasia and America), biomes (i.e. boreal and tundra), permafrost conditions (i.e. continuous, discontinuous, and permafrost-free), and observational scales (i.e. 1 km, 2 km, 4 km, and 8 km).

conversions between surface water and vegetation condition in focal locations. This interpretation is indeed in line with remote sensing and *in situ* observations showing direct conversions between woody vegetation and surface water cover across a wide geographic range including many areas in western and eastern Siberia (Crawford *et al* 2003, Kirpotin *et al* 2009, Iwasaki *et al* 2010, Moskalenko 2013, Miles and Esau 2016), as well as in Alaska (Arp *et al* 2011, Jones *et al* 2011, Raynolds *et al* 2014, Nitze and Grosse 2016, Raynolds and Walker 2016, Lara *et al* 2018). Empirical evidence has also been obtained from local-scale experiments in northeastern Siberian tundra showing that where shrub canopy has been removed ponds quickly form (Nauta *et al* 2015).

Interestingly, our further analysis reveals that when a particular focal area experienced a decreasing trend of surface water cover, its neighboring terrestrial areas tended to exhibit spectral greening (figures S5–S7). The association of changes was also evident in the opposite direction as spectral browning increased adjacent to newly formed water bodies (figures S5–S7). These neighborhood associations suggest the existence of 'spillover effects' (i.e. a spatial process by which changes in a particular area can cascade to induce changes in nearby areas) (LeSage and Pace 2009). We used spatial regression modeling to infer if such neighboring associations could be purely attributed to a SA process (i.e. where certain external environmental factors drive both greenness and surface water cover trends, thus giving rise to their associations, a process referred to as extrinsic SA (Teng *et al* 2018); see section 2 and supplementary materials section S1). Our results suggest that the observed associations are not solely caused by extrinsic SA. Instead, we found signs that changes in both spectral greenness and surface water cover at focal sites can spill over to produce significant influences on land cover changes in neighboring areas (figure S8), suggesting that vegetation condition and surface water cover plausibly interact with each other.

3.2. Inference of vegetation-water interactions

The SEM suggests that overall the associated trends of spectral greenness and surface water cover are better explained by bi-directional relationships, in which spectral greenness and surface water cover trends influence each other. In some situations, the performance of this bi-directional model may not exceed the results assuming one-way effects of surface water cover on spectral greenness (see figure 2(c) for the model structure and table S2 for results depending on continent, vegetation type and permafrost condition, as well as type of vegetation index and trend indicator used). We also observed a negative effect of topographic slope on water cover trend (figure 2(c)), in line with the well-known effect of slower drainage in flat areas facilitating water accumulation and increases in surface water cover. However, the effects of topographic condition and climate (i.e. MAT and MAP) trends, on changes in surface water cover, were much weaker than the inferred vegetation-water interactions, echoing the highlighted complexity of soil and surface water changes in response to climate warming and permafrost thawing in northern high latitudes (Walvoord and Kurylyk 2016).

3.3. Possible mechanisms

These revealed associations between changes in spectral greenness and surface water cover could be explained by several mechanisms. For example, increasing waterlogged conditions resulting in increases in surface water cover can elevate mortality of trees and shrubs as reported in lowland boreal forests and tundra across Alaska, Canada, and northern Eurasia (Forbes *et al* 2010). Loss of woody cover may exacerbate summer thawing of permafrost, further increasing surface water cover (Blok *et al* 2010, Nauta *et al* 2015).

Interestingly, bi-directional relationships appear to be mostly associated to regions with continuous permafrost where soil ice content is high (table S2). This is in line with the suggested feedback between permafrost thawing and vegetation cover loss (Blok *et al* 2010, Nauta *et al* 2015). If permafrost condition indeed underlies the direction of vegetation-water interactions, one would expect to observe this bi-directional pattern more commonly in regions where permafrost is more abundant. In line with this, we found more pronounced bi-directional relationships in the tundra biome dominated by continuous permafrost than in the more southern boreal biome (table S2). We also found more pronounced bi-directional relationships between trends in surface water cover and spectral greenness in Eurasia (whereas one-way in North America, as suggested by the SEM fitting). This continental difference could be attributed to the larger fraction of continuous permafrost in Eurasia than in North America (Brown *et al* 2002) as well as the stronger heatwaves occurring in Eurasia (Schubert *et al* 2014).

Despite the dominant negative correlation between trends of spectral greenness and surface water cover, it is not uncommon to find positive associations in particular areas scattered across the boreal and tundra biomes. In relatively dry areas within a landscape, increasing surface water can alleviate limitation of soil water and facilitate vegetation growth (Ruiz-Pérez and Vico 2020, Sungmin *et al* 2020). Also, in wetlands, the productivity of wetland-adapted plants may increase with warming and CO_2 fertilization, resulting in greenness increases along with increases in surface water cover induced by permafrost thawing (Park *et al* 2016). On the other hand, drier soils resulting from surface water drainage (Smith *et al* 2005, Hinkel *et al* 2007, Marsh *et al* 2009) can facilitate the replacement of sedges and mosses by shrubs and trees (Frohn *et al* 2005, Jorgenson *et al* 2013, Li *et al* 2017) and enhance tree growth (Ropars *et al* 2015). In turn, positive interactions between shrubs and trees can reinforce woody plant encroachment and succession (Holmgren *et al* 2015, Limpens *et al* 2021), increasing water transport from soil to atmosphere and further contributing to reductions in soil water and surface water cover (Waddington *et al* 2015).

While soil moisture has been shown to correlate with Arctic greening (Berner *et al* 2020), the explicit link between surface water and vegetation change has been poorly explored using remote sensing as surface water bodies are often excluded to prevent confounding factors. Given the significant complexity and heterogeneity of ecosystem processes in northern high latitudes, we do not expect that the inferred interactions between vegetation and surface water changes are ubiquitous at the biome-wide scale. However, they may at least partly explain why both greening and browning have been observed across the boreal and tundra biomes. These interactions between vegetation condition and water cover may alter carbon dynamics and biogeochemical cycles. Vegetation browning may result in loss of stored above-ground and below-ground carbon as permafrost thaws and stored organic matter decomposes (Walter *et al* 2006, Schuur *et al* 2015). In well drained areas, reduction of surface and soil water may also lead to enhanced decomposition and increase CO_2 and methane release (Natali *et al* 2015). On the other hand, while vegetation greening can partly compensate for the loss of stored carbon, it may also further stimulate decomposition of native soil carbon (Fontaine *et al* 2003).

3.4. Caveats and limitations

We cannot rule out the possibility that intrinsic limitations of current remote sensing tools may influence the observed patterns to some extent. For example, 'gridding artifacts' (Tan *et al* 2006) denote that nearby water pixels can contribute to the reflectance of the focal vegetated pixel. Sufficiently strong gridding artifacts thus can result in spectral browning positively correlated with increasing cover of surface water. However, if the gridding artifacts were fully responsible for the surface water-browning pattern, one would expect to observe clear differences between MODIS and Landsat data. Yet, both remote sensing tools detect the same patterns (figure S3).

Another technical caveat to keep in mind is the influence of subpixel heterogeneity, which is inevitable at medium to coarse spatial resolutions. The probability that focal pixels are partly covered by surface water probably increases and leads to spectral browning if neighboring pixels exhibit a positive trend of surface water cover and/or are largely covered by surface water. However, if the observed negative trend associations were largely an artefact resulting from subpixel heterogeneity, Landsat data that are less prone to subpixel heterogeneity would have given weaker trend correlations than the MODIS data. Yet, the results from MODIS and Landsat data are consistent with each other (table S1).

Despite that our observed patterns are unlikely resulting from pure remote sensing artifacts, the abovementioned caveats should be taken into account for further unraveling vegetation-water interactions in the northern high latitude regions using remote sensing data. The increasing availability of high-resolution remote sensing datasets at multiple temporal coverages and enhanced computation power of cloud computation platforms may help overcoming the current technical limitations of coarse- and moderate-resolution remote sensing tools.

4. Conclusions

Taken together, our analyses reveal clear associations between divergent changes in surface water cover and spectral greening and browning. These changes we infer may also create positive feedback loops that self-reinforce changes in vegetation, permafrost thawing and surface water at relatively small spatial scales. In local areas where these feedbacks are strong enough, they may effectively reinforce or offset the direct effects of climate changes on permafrost thawing and vegetation. While it is impossible to rigorously verify the existence and quantify the intensity of these feedbacks globally with correlational evidence only, our results convey the important message that changes in surface water could play a critical (but largely neglected) role in ecosystem structure and functioning at northern high latitudes. Our results thus imply that the recent projections of abrupt permafrost degradation across northern high latitudes (Teufel and Sushama 2019) can be locally reinforced by local interactions between water and vegetation (Scheffer *et al* 2012). This may help to explain the existence of abrupt vegetation states reported earlier across the boreal and tundra biomes (Scheffer *et al* 2012, Xu *et al* 2015, Teufel and Sushama 2019). Searching for abrupt changes in VI time series using methods such as the breaks for additive seasonal and trend method (Verbesselt *et al* 2010) may help to better foresee if and to what extent biome-wide tipping points could occur in the future.

Our findings have major implications globally. Climate warming is expected to increase permafrost thawing. The accumulation of inland surface water as a consequence, especially in Arctic and sub-Arctic regions with low drainage, will likely increase the extent of wetlands, changing ecological communities, biogeochemical cycles and their feedback to the climate system. This process could be accelerated in regions where warming is also combined with higher rainfall levels or stronger pulses of precipitation events as our planet warms up. We expect therefore that vegetation browning may be amplified in many regions across the northern high latitudes. To monitor the changes we expect and assess the mechanisms we propose here, it will be important to combine high resolution remote sensing with field experiments at larger spatial extents that currently undertaken to unraveling the complex interactions between climate, vegetation cover, snow accumulation, permafrost condition, hydrology and albedo. Simulation models that adequately account for these interactions may help to better project the responses of these massive ecosystems to climate change.

Data availability

All data used in this study are publicly available. The MODIS NDVI and EVI data are available at https://lpdaac.usgs.gov/products/mod13q1v006/. The Landsat NDVI and EVI data are available at https://developers.google.com/earth-engine/datasets/catalog/LANDSAT_LE07_C01_T1_SR. The water cover data are available at https://global-surface-water.appspot.com/download. The MAT and MAP data are available at the CRU (www.cru.uea.acuk/data). The permafrost data are available at https://nsidc.org/data/ggd318. The elevation data are available at www.usgs.gov/centers/eros/science/usgs-eros-archive-digital-elevation-global-30-arc-second-elevation-gtopo30.

All data that support the findings of this study are included within the article (and any supplementary files).

Acknowledgments

We thank Marten Scheffer and three anonymous reviewers for valuable suggestions to earlier versions of this manuscript. We also thank Jean-François Pekel and Shuqing Teng for advice on water data processing and spatial regression modeling, respectively. This study was funded by the National Natural Science Foundation of China (NSFC 32061143014 and 31770512). J L is supported by the China Scholarship Council and Wageningen University (NL).

Author contributions

C X and M H designed the research, J L conducted the analyses, C X and M H wrote the first draft and supervised all stages of this work. All authors contributed to interpreting and revising the text.

Conflict of interest

The authors declare no competing interests.

ORCID iD

Chi Xu https://orcid.org/0000-0002-1841-9032

References

Arp C D, Jones B M, Urban F E and Grosse G 2011 Hydrogeomorphic processes of thermokarst lakes with grounded-ice and floating-ice regimes on the Arctic coastal plain, AK *Hydrol. Process.* **25** 2422–38

Beck P S, Juday G P, Alix C, Barber V A, Winslow S E, Sousa E E, Heiser P, Herriges J D and Goetz S J 2011 Changes in forest productivity across Alaska consistent with biome shift *Ecol. Lett.* **14** 373–9

Berner L T *et al* 2020 Summer warming explains widespread but not uniform greening in the Arctic tundra biome *Nat. Commun.* **11** 4621

Bjerke J W, Treharne R, Vikhamar-Schuler D, Karlsen S R, Ravolainen V, Bokhorst S, Phoenix G K, Bochenek Z and Tømmervik H 2017 Understanding the drivers of extensive plant damage in boreal and Arctic ecosystems: insights from field surveys in the aftermath of damage *Sci. Total Environ.* **599** 1965–76

Blok D, Heijmans M M, Schaepman-Strub G, Kononov A, Maximov T and Berendse F 2010 Shrub expansion may reduce summer permafrost thaw in Siberian tundra *Glob. Change Biol.* **16** 1296–305

Bokhorst S, Bjerke J W, Street L, Callaghan T V and Phoenix G K 2011 Impacts of multiple extreme winter warming events on sub-Arctic heathland: phenology, reproduction, growth, and CO_2 flux responses *Glob. Change Biol.* **17** 2817–30

Bret-Harte M S, Mack M C, Shaver G R, Huebner D C, Johnston M, Mojica C A, Pizano C and Reiskind J A 2013 The response of Arctic vegetation and soils following an unusually severe tundra fire *Phil. Trans. R. Soc.* B **368** 20120490

Brown J, Ferrians O Jr, Heginbottom J and Melnikov E 2002 *Circum-Arctic Map of Permafrost and Ground-Ice Conditions, Version 2* (Boulder, CO: NSIDC: National Snow and Ice Data Center)

Crawford R, Jeffree C and Rees W 2003 Paludification and forest retreat in northern oceanic environments *Ann. Bot.* **91** 213–26

Didan K 2015 *MOD13Q1 MODIS/Terra Vegetation Indices 16-day L3 Global 250 m SIN Grid V006* (NASA EOSDIS Land Processes DAAC)

Elmendorf S C *et al* 2012 Plot-scale evidence of tundra vegetation change and links to recent summer warming *Nat. Clim. Change* **2** 453–7

Fontaine S, Mariotti A and Abbadie L 2003 The priming effect of organic matter: a question of microbial competition? *Soil Biol. Biochem.* **35** 837–43

Forbes B C, Fauria M M and Zetterberg P 2010 Russian Arctic warming and 'greening' are closely tracked by tundra shrub willows *Glob. Change Biol.* **16** 1542–54

Frohn R C, Hinkel K M and Eisner W R 2005 Satellite remote sensing classification of thaw lakes and drained thaw lake basins on the North Slope of Alaska *Remote Sens. Environ.* **97** 116–26

Frost G V and Epstein H E 2014 Tall shrub and tree expansion in Siberian tundra ecotones since the 1960s *Glob. Change Biol.* **20** 1264–77

Gamon J A, Huemmrich K F, Stone R S and Tweedie C E 2013 Spatial and temporal variation in primary productivity (NDVI) of coastal Alaskan tundra: decreased vegetation growth following earlier snowmelt *Remote Sens. Environ.* **129** 144–53

Giglio L, Justice C, Boschetti L and Roy D 2015 *MCD64A1 MODIS/Terra+ Aqua Burned Area Monthly L3 Global 500 m SIN Grid V006 [Data Set]* (Sioux Falls, SD: NASA EOSDIS Land Processes DAAC)

Goetz S J, Bunn A G, Fiske G J and Houghton R A 2005 Satellite-observed photosynthetic trends across boreal North America associated with climate and fire disturbance *Proc. Natl Acad. Sci.* **102** 13521–5

Gorelick N, Hancher M, Dixon M, Ilyushchenko S, Thau D and Moore R 2017 Google Earth Engine: planetary-scale geospatial analysis for everyone *Remote Sens. Environ.* **202** 18–27

Guay K C, Beck P S, Berner L T, Goetz S J, Baccini A and Buermann W 2014 Vegetation productivity patterns at high northern latitudes: a multi-sensor satellite data assessment *Glob. Change Biol.* **20** 3147–58

Guindon L, Bernier P, Gauthier S, Stinson G, Villemaire P and Beaudoin A 2018 Missing forest cover gains in boreal forests explained *Ecosphere* **9** e02094

Harris I, Osborn T J, Jones P and Lister D 2020 Version 4 of the CRU TS monthly high-resolution gridded multivariate climate dataset *Sci. Data* **7** 109

Hinkel K M, Jones B M, Eisner W R, Cuomo C J, Beck R A and Frohn R 2007 Methods to assess natural and anthropogenic thaw lake drainage on the western Arctic coastal plain of northern Alaska *J. Geophys. Res.: Earth Surf.* **112** F02S16

Hinzman L D *et al* 2005 Evidence and implications of recent climate change in northern Alaska and other arctic regions *Clim. Change* **72** 251–98

Holmgren M *et al* 2015 Positive shrub–tree interactions facilitate woody encroachment in boreal peatlands *J. Ecol.* **103** 58–66
Iwasaki H, Saito H, Kuwao K, Maximov T and Hasegawa S 2010 Forest decline caused by high soil water conditions in a permafrost region *Hydrol. Earth Syst. Sci.* **14** 301–7
Jones B M, Grosse G, Arp C, Jones M, Anthony K W and Romanovsky V 2011 Modern thermokarst lake dynamics in the continuous permafrost zone, northern Seward Peninsula, AK *J. Geophys. Res.: Biogeosci.* **116** G00M03
Jorgenson M T *et al* 2013 Reorganization of vegetation, hydrology and soil carbon after permafrost degradation across heterogeneous boreal landscapes *Environ. Res. Lett.* **8** 035017
Karlsson J M, Bring A, Peterson G D, Gordon L J and Destouni G 2011 Opportunities and limitations to detect climate-related regime shifts in inland Arctic ecosystems through eco-hydrological monitoring *Environ. Res. Lett.* **6** 014015
Kirpotin S N *et al* 2009 Western Siberia wetlands as indicator and regulator of climate change on the global scale *Int. J. Environ. Stud.* **66** 409–21
Lara M J, Nitze I, Grosse G, Martin P and McGuire A D 2018 Reduced Arctic tundra productivity linked with landform and climate change interactions *Sci. Rep.* **8** 2345
Lefcheck J S 2016 PiecewiseSEM: piecewise structural equation modelling in R for ecology, evolution, and systematics *Methods Ecol. Evol.* **7** 573–9
LeSage J and Pace R K 2009 *Introduction to Spatial Econometrics* (Boca Raton, FL: CRC Press)
Li B, Heijmans M M, Blok D, Wang P, Karsanaev S V, Maximov T C, van Huissteden J and Berendse F 2017 Thaw pond development and initial vegetation succession in experimental plots at a Siberian lowland tundra site *Plant Soil* **420** 147–62
Limpens J *et al* 2021 Shrubs and degraded permafrost pave the way for tree establishment in subarctic peatlands *Ecosystems* **24** 370–83
Macias-Fauria M, Seddon A W, Benz D, Long P R and Willis K 2014 Spatiotemporal patterns of warming *Nat. Clim. Change* **4** 845–6
Marsh P, Russell M, Pohl S, Haywood H and Onclin C 2009 Changes in thaw lake drainage in the Western Canadian Arctic from 1950 to 2000 *Hydrol. Process.* **23** 145–58
Miles V V and Esau I 2016 Spatial heterogeneity of greening and browning between and within bioclimatic zones in northern West Siberia *Environ. Res. Lett.* **11** 115002
Moskalenko N 2013 Impact of climate warming on vegetation cover and permafrost in West Siberia northern taiga *Nat. Sci.* **5** 144–8
Myers-Smith I H *et al* 2020 Complexity revealed in the greening of the Arctic *Nat. Clim. Change* **10** 106–17
Myneni R B, Keeling C, Tucker C J, Asrar G and Nemani R R 1997 Increased plant growth in the northern high latitudes from 1981 to 1991 *Nature* **386** 698–702
Natali S M *et al* 2015 Permafrost thaw and soil moisture driving CO_2 and CH_4 release from upland tundra *J. Geophys. Res.: Biogeosci.* **120** 525–37
National Academies Of Sciences E 2019 *Understanding Northern Latitude Vegetation Greening and Browning: Proceedings of a Workshop* (Washington, DC: The National Academies Press)
Nauta A L *et al* 2015 Permafrost collapse after shrub removal shifts tundra ecosystem to a methane source *Nat. Clim. Change* **5** 67–70
Nitze I and Grosse G 2016 Detection of landscape dynamics in the Arctic Lena Delta with temporally dense Landsat time-series stacks *Remote Sens. Environ.* **181** 27–41
Olson D M *et al* 2001 Terrestrial ecoregions of the world: a new map of life on Earth a new global map of terrestrial ecoregions provides an innovative tool for conserving biodiversity *BioScience* **51** 933–8
Osterkamp T, Viereck L, Shur Y, Jorgenson M, Racine C, Doyle A and Boone R 2000 Observations of thermokarst and its impact on boreal forests in AK, USA *Arct. Antarct. Alp. Res.* **32** 303–15
Pachauri R K *et al* 2014 Climate change 2014: synthesis report *Contribution of Working Groups I, II and III to the 5th assessment report of the Intergovernmental Panel on Climate Change* (IPCC)
Park T, Ganguly S, Tømmervik H, Euskirchen E S, Høgda K-A, Karlsen S R, Brovkin V, Nemani R R and Myneni R B 2016 Changes in growing season duration and productivity of northern vegetation inferred from long-term remote sensing data *Environ. Res. Lett.* **11** 084001
Pekel J-F, Cottam A, Gorelick N and Belward A S 2016 High-resolution mapping of global surface water and its long-term changes *Nature* **540** 418–22
Phoenix G K and Bjerke J W 2016 Arctic browning: extreme events and trends reversing arctic greening *Glob. Change Biol.* **22** 2960–2
Piao S *et al* 2020 Characteristics, drivers and feedbacks of global greening *Nat. Rev. Earth Environ.* **1** 14–27
Post E *et al* 2019 The polar regions in a 2 °C warmer world *Sci. Adv.* **5** eaaw9883
R Core Team 2018 R: a language and environment for statistical computing (Vienna: R Foundation for Statistical Computing) (available at: www.R-project.org/ (Accessed 26 May 2020))
Raynolds M K *et al* 2014 Cumulative geoecological effects of 62 years of infrastructure and climate change in ice-rich permafrost landscapes, Prudhoe Bay Oilfield, AK *Glob. Change Biol.* **20** 1211–24
Raynolds M K and Walker D A 2016 Increased wetness confounds Landsat-derived NDVI trends in the central Alaska North Slope region, 1985–2011 *Environ. Res. Lett.* **11** 085004
Ropars P, Lévesque E and Boudreau S 2015 How do climate and topography influence the greening of the forest-tundra ecotone in northern Québec? A dendrochronological analysis of Betula glandulosa *J. Ecol.* **103** 679–90
Ruiz-Pérez G and Vico G 2020 Effects of temperature and water availability on Northern European boreal forests *Front. For. Glob. Change* **3** 34
Scheffer M, Hirota M, Holmgren M, van Nes E H and Chapin F S III 2012 Thresholds for boreal biome transitions *Proc. Natl Acad. Sci.* **109** 21384–9
Schubert S D, Wang H, Koster R D, Suarez M J and Groisman P Y 2014 Northern Eurasian heat waves and droughts *J. Clim.* **27** 3169–207
Schuur E A *et al* 2015 Climate change and the permafrost carbon feedback *Nature* **520** 171–9
Smith L C, Sheng Y, MacDonald G and Hinzman L 2005 Disappearing Arctic lakes *Science* **308** 1429
Sturm M, Holmgren J, McFadden J P, Liston G E, Chapin F S III and Racine C H 2001 Snow–shrub interactions in Arctic tundra: a hypothesis with climatic implications *J. Clim.* **14** 336–44
Sungmin O, Hou X and Orth R 2020 Observational evidence of wildfire-promoting soil moisture anomalies *Sci. Rep.* **10** 11008
Tan B, Woodcock C, Hu J, Zhang P, Ozdogan M, Huang D, Yang W, Knyazikhin Y and Myneni R 2006 The impact of gridding artifacts on the local spatial properties of MODIS data: implications for validation, compositing, and band-to-band registration across resolutions *Remote Sens. Environ.* **105** 98–114
Teng S N, Xu C, Sandel B and Svenning J C 2018 Effects of intrinsic sources of spatial autocorrelation on spatial regression modelling *Methods Ecol. Evol.* **9** 363–72
Teufel B and Sushama L 2019 Abrupt changes across the Arctic permafrost region endanger northern development *Nat. Clim. Change* **9** 858–62
Verbesselt J, Hyndman R, Newnham G and Culvenor D 2010 Detecting trend and seasonal changes in satellite image time series *Remote Sens. Environ.* **114** 106–15
Waddington J, Morris P, Kettridge N, Granath G, Thompson D and Moore P 2015 Hydrological feedbacks in northern peatlands *Ecohydrology* **8** 113–27

Walter K M, Zimov S A, Chanton J P, Verbyla D and Chapin F S III 2006 Methane bubbling from Siberian thaw lakes as a positive feedback to climate warming *Nature* **443** 71–75

Walvoord M A and Kurylyk B L 2016 Hydrologic impacts of thawing permafrost—a review *Vadose Zone J.* **15** 1–20

Wang J A and Friedl M A 2019 The role of land cover change in Arctic-boreal greening and browning trends *Environ. Res. Lett.* **14** 125007

Wildlife Conservation Society—WCS and Center for International Earth Science Information Network—CIESIN—Columbia University 2005 *Last of the Wild Project, Version 2, 2005 (LWP-2): Global Human Influence Index (HII) Dataset (Geographic)* (Palisades, NY: NASA Socioeconomic Data and Applications Center (SEDAC))

Xu C, Holmgren M, van Nes E H, Hirota M, Chapin F S III and Scheffer M 2015 A changing number of alternative states in the boreal biome: reproducibility risks of replacing remote sensing products *PLoS One* **10** e0143014

Zeng H, Jia G and Forbes B C 2013 Shifts in Arctic phenology in response to climate and anthropogenic factors as detected from multiple satellite time series *Environ. Res. Lett.* **8** 035036